addition of polarization data, which enter into the ISW detection levels mentioned above through the *Planck* lensing map.

Since a purely gravitational effect does not polarize photons, polarization data in principle provide a powerful discriminant between ISW and primary CMB fluctuations. The current *Planck* polarization maps, however, are not usable at the largest scales (Sect. 2.2), so this tool cannot yet be fully exploited.

Polarization data on smaller scales ($\gtrsim 5^\circ$) can be used to probe the ISW effect through stacking of CMB anisotropies at the positions of known superstructures. We have studied the photometric profiles of *Planck* CMB polarization patches at the locations of the Granett et al. (2008) catalogue of superclusters and super-voids, which have been reported as anomalous ISW sources (e.g., Planck Collaboration XVII 2014). Our analysis, using specially-constructed CMB temperature maps that are correlated and uncorrelated with $E$-modes, cannot rule out the ISW effect as the cause of these anomalies.

A map of the ISW anisotropies is presented in Fig. 21. It shows the redshifts and blueshifts suffered by CMB photons travelling through the gravitational potential traced by different galaxy catalogues and the *Planck* lensing map. Our reconstruction has a mean error of $\approx 15$ $\mu$K (per roughly $1^\circ$ pixel).

### 10.9. Cosmology from clusters

In 2013 we found an apparent tension between our primary CMB constraints and those from the *Planck* cluster counts, with the clusters preferring a lower normalization of the matter power spectrum, $\sigma_8$. The comparison is interesting because the cluster counts directly measure $\sigma_8$ at low redshift and hence any tension could signal the need for extensions of the base model, such as non-minimal neutrino mass. However, limited knowledge of the normalization of the scaling relation between SZ signal and mass (usually called "mass bias") continues to hamper the interpretation of this result.

Our 2015 cluster analysis benefits from a larger catalogue (438 objects versus the 189 in 2013), greater control of the selection function, and recent gravitational lensing determinations of the mass bias for *Planck* clusters. With the larger sample, we now fit the counts in the 2-dimensional plane of redshift and S/N, allowing us to simultaneously constrain the slope of the scaling relation and the cosmological parameters. We examine three new empirical determinations of the mass bias from gravitational lensing: weighing the Giants (WtG; von der Linden et al. 2014); the Canadian Cluster Comparison Project (CCCP; Hoekstra et al., priv. comm.); and results from a new method based on CMB lensing (Melin & Bartlett 2015). We use these three results as priors because they measure the mass scale directly on samples of *Planck* clusters.

The cluster constraints on $\sigma_8$ and $\Omega_m$ are statistically identical to those of 2013 when adopting the same scaling relation and mass bias; in this sense, we confirm the 2013 results with the larger 2015 catalogue. Applying the three new mass bias priors, we find that the WtG calibration reduces the tension with the primary CMB constraints to slightly more than $1\sigma$ in the base model, and CCCP results in tension at just over $2\sigma$, similar to the case for the CMB lensing calibration. More detailed discussion of constraints from *Planck* cluster counts can be found in Planck Collaboration XXIV (2016).

## 11. *Planck* 2015 astrophysics results

### 11.1. Low frequency foregrounds

Galactic foreground emission between 20 and 100 GHz, based primarily on the `Commander` component separation of Planck Collaboration X (2016), is discussed in Planck Collaboration XXV (2016). The total intensity in this part of the spectrum is dominated by free-free and spinning dust emission, while polarization is dominated by synchrotron emission.

Comparison with radio recombination line templates verifies the recovery of the free-free emission along the Galactic plane. Comparison of high-latitude H$\alpha$ emission with our free-free map shows residuals that correlate with dust optical depth, consistent with a fraction (around 30%) of H$\alpha$ having been scattered by high-latitude dust. A number of diffuse morphological features of spinning dust at high latitude can be highlighted. There is substantial spatial variation in the spinning dust spectrum, with the emission peak (in $I_\nu$) ranging from below 20 GHz to more than 50 GHz. There is a strong tendency for the spinning dust component near prominent H II regions to have a higher peak frequency, suggesting that this increase in peak frequency is associated with dust in the photo-dissociation regions around the nebulae. The emissivity of spinning dust in these diffuse regions is of the same order as previous detections in the literature. Over the entire sky, the `Commander` solution finds more anomalous microwave emission (AME) than the WMAP component maps, at the expense of synchrotron and free-free emission. Although the `Commander` model fits the data exceptionally well, as noted in Sect 9.4, the discrepancy is largely driven by differences in the assumed synchrotron spectrum and the more elaborate model of spinning dust designed to allow for the variation in peak frequency noted above. Future surveys, particularly at 5–20 GHz, will greatly improve the separation, since the predicted brightness between the two models disagrees substantially in that range.

In polarization, synchrotron emission completely dominates on angular scales larger than $1^\circ$ and frequencies up to 44 GHz. We combine *Planck* and WMAP data to make the highest signal-to-noise ratio map yet of the intensity of the all-sky polarized synchrotron emission at frequencies above a few gigahertz, where Faraday rotation and depolarization are negligible (Figs. 22 and 23). Most of the high-latitude polarized emission is associated with distinct large-scale loops and spurs, and we rediscuss their structure following the earlier study of Vidal et al. (2015) based on WMAP observations. We argue that nearly all the emission at $-90^\circ < l < 40^\circ$ is part of the Loop I structure, and show that the emission extends much further into the southern Galactic hemisphere than previously recognized, giving Loop I an ovoid rather than circular outline. However, it does not continue as far as the "*Fermi* bubble/microwave haze", which probably rules out an association between the two structures. The South Polar Spur (SPS, see Fig. 22) is bordered by a polarized dust filament and associated low-velocity H I emission, analogous to the cold features long known to border Loop I around the North Polar Spur. We find two structures that could correspond to distant analogues of the radio loops, as predicted by Mertsch & Sarkar (2013), including one surrounding the Cygnus X star-forming region, both of which are again associated with dust polarization.

We identify a number of other faint features in the polarized sky, including a dearth of polarized synchrotron emission directly correlated with a narrow, $20^\circ$-long filament seen in H$\alpha$ at high Galactic latitude, and also visible in the Faraday rotation map of Oppermann et al. (2012). Finally, we look for evidence of

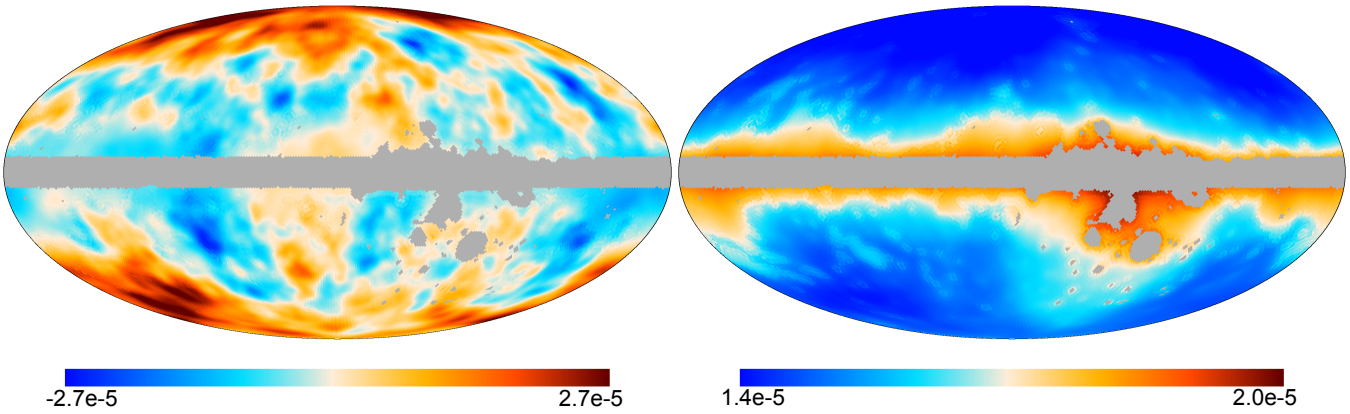


**Fig. 21.** Maps of ISW anisotropies (*left*) and their (per pixel) uncertainties (*right*), from the combination of the *Planck* SEVEM CMB map and the large-scale structure tracers used in Planck Collaboration XXI (2016): NVSS; WISE galaxies and AGN; and luminous photometrically-selected galaxies from SDSS. The units are kelvins.

polarized AME. Many AME regions, however, are significantly contaminated by polarized synchrotron emission, and we find a $2\sigma$ upper limit of 1.6% in the Perseus region.

### *11.2. Polarized thermal dust emission*

*Planck* has produced the first all-sky map of the polarized emission from dust at submillimetre wavelengths (Figs. 17 and 24). Compared with earlier ground-based and balloon-borne observations (e.g., Benoît et al. 2004; Ward-Thompson et al. 2009; Matthews et al. 2009, 2014; Koch et al. 2010) this survey is an immense step forward in sensitivity, coverage, and statistics. It provides new insight into the structure of the Galactic magnetic field and the properties of dust, as well as the first statistical characterization of one of the main foregrounds to CMB polarization. The wealth of information encoded in the all-sky maps of polarized intensity, $P$, polarization fraction, $p$, and polarization angle, $\psi$, presented in Planck Collaboration X (2016), is illustrated in Fig. 25. Here we summarize the main results from the data analysis by the Planck Consortium. The release of the data to the science community at large will trigger many more studies.

#### 11.2.1. The dust polarization sky

Planck Collaboration Int. XIX (2015) presents an overview of the polarized sky as seen by *Planck* at 353 GHz (the most sensitive *Planck* channel for polarized thermal dust emission), focusing on the statistics of $p$ and $\psi$. At all $N_{\rm H}$ below $10^{22}$ cm$^{-2}$, $p$ displays a large scatter. The maximum $p$, observed in regions of moderate hydrogen column density ($N_{\rm H} < 2{\times}10^{21}$ cm$^{-2}$), is high ($p_{\rm max} \approx 20\%$). There is a general decrease in $p$ with increasing column density above $N_{\rm H} \approx 1 \times 10^{21}$ cm$^{-2}$ and in particular a sharp drop above $N_{\rm H} \approx 10^{22}$ cm$^{-2}$.

The spatial structure of $\psi$ is characterized using the angle dispersion function $\mathcal{S}$, the local dispersion of $\psi$ (introduced by Hildebrand et al. 2009). The polarization fraction is found to be anti-correlated with $\mathcal{S}$. The polarization angle is ordered over extended areas of several square degrees. The ordered areas are separated by long, narrow structures of high $\mathcal{S}$ that highlight interfaces where the sky polarization changes abruptly. These structures have no clear counterpart in the map of the total intensity, $I$. They bear a morphological resemblance to features detected in gradient maps of radio polarized emission (Iacobelli et al. 2014).

#### 11.2.2. The Galactic magnetic field

The *Planck* maps of $p$ and $\psi$ contain information on the magnetic field structure. The data have been compared to synthetic polarized emission maps computed from simulations of anisotropic magnetohydrodynamical turbulence, assuming simply a uniform intrinsic polarization fraction of dust grains (Planck Collaboration Int. XX 2015). The turbulent structure of the magnetic field is able to reproduce the main statistical properties of $p$ and $\psi$ that are observed directly in a variety of nearby clouds (dense cores excluded). The large-scale field orientation with respect to the line of sight plays a major role in the quantitative analysis of these statistical properties. This study suggests that the large scatter of $p$ at $N_{\rm H}$ smaller than about $10^{22}$ cm$^{-2}$ is due mainly to fluctuations in the magnetic field orientation along the line of sight, rather than to changes in grain shape and/or the efficiency of grain alignment.

The formation of density structures in the interstellar medium involves turbulence, gas cooling, magnetic fields, and gravity. Polarization of thermal dust emission is well suited to studying the role of the magnetic field, because it images structure through an emission process that traces the mass of interstellar matter (Planck Collaboration XI 2014). The *Planck* $I$ map shows elongated structures (filaments or ridges) that have counterparts in either the Stokes $Q$ or $U$ map, or in both, depending on the mean orientation. The correlation between Stokes maps characterizes the relative orientation between the ridges and the magnetic field. In the diffuse interstellar medium, the ridges are preferentially aligned with the magnetic field measured on the structures. This statistical trend becomes more striking for decreasing column density and, as expected from the potential effects of projection, for increasing polarization fraction (Planck Collaboration Int. XXXII 2016). Towards nearby molecular clouds the relative orientation changes progressively from preferentially parallel in areas with the lowest $N_{\rm H}$ to preferentially perpendicular in the areas with the highest $N_{\rm H}$ (Planck Collaboration Int. XXXV 2016). This change in relative orientation might be a signature of the formation of gravitationally-bound structures in the presence of a dynamically-important magnetic field.

The relation between the structure of matter and the magnetic field is also investigated in Planck Collaboration Int. XXXIII (2016) through modelling of the variations of the Stokes parameters across three filaments for different hypotheses on $p$. For these representative structures in molecular clouds, the

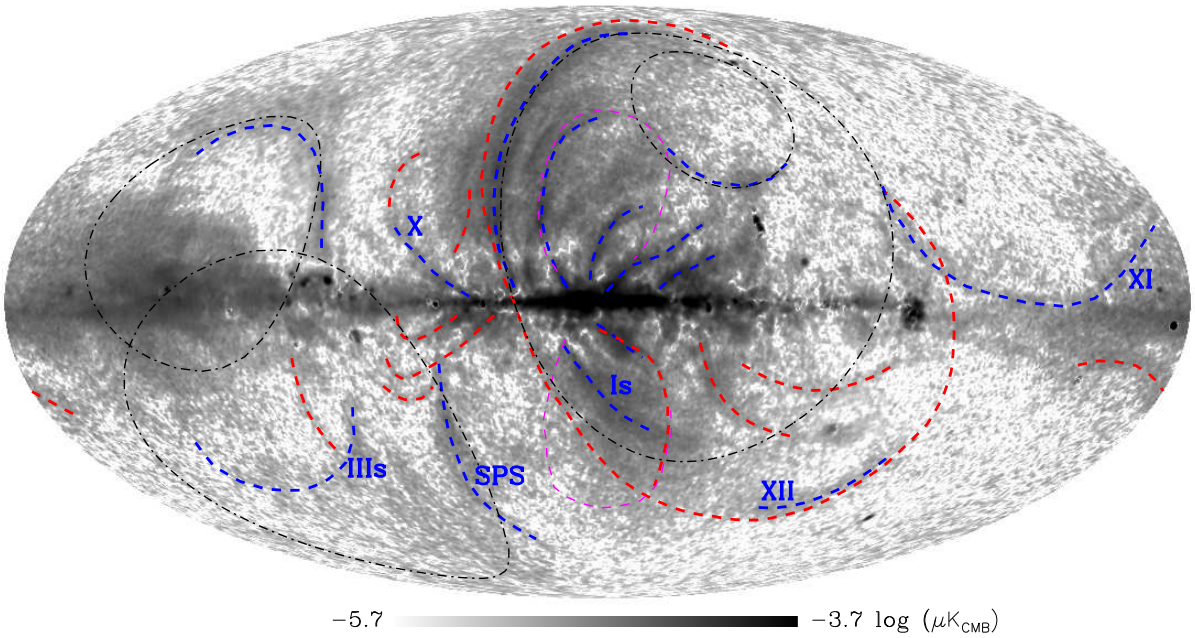


**Fig. 22.** Synchrotron polarization amplitude map, $P = \sqrt{Q^2 + U^2}$, at 30 GHz, smoothed to an angular resolution of 60′, produced by a weighted sum of *Planck* and WMAP data as described in Planck Collaboration XXV (2016). The traditional locii of radio loops I–IV are marked in black, a selection of the spurs identified by Vidal et al. (2015) in blue, the outline of the *Fermi* bubbles in magenta, and features discussed for the first time in Planck Collaboration XXV (2016) in red. Our measured outline for Loop I departs substantially from the traditional small circle.

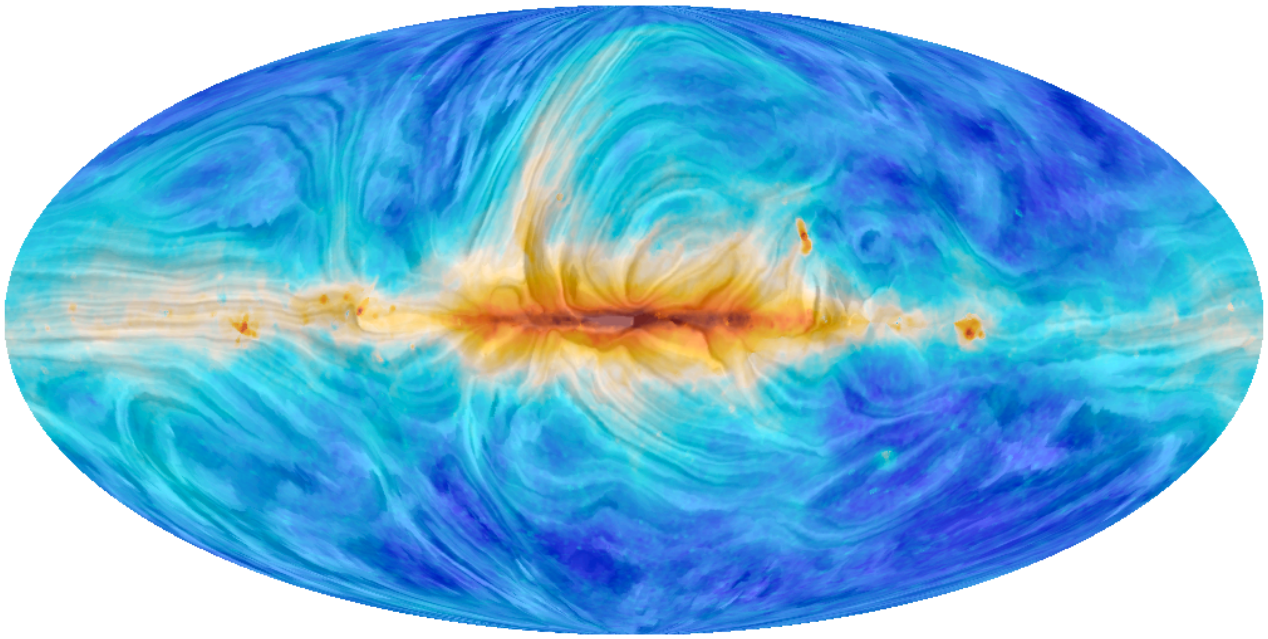

**Fig. 23.** All-sky view of the angle of polarization at 30 GHz, rotated by 90° to indicate the direction of the Galactic magnetic field projected on the plane of the sky. The colours represent intensity, dominated at this frequency by synchrotron emission. The "drapery" pattern was obtained by applying the line integral convolution (LIC; Cabral & Leedom 1993) procedure using an IDL implementation provided by Diego Falceta-Gonçalves (http://each.uspnet.usp.br/fgoncalves/pros/lic.pro). This gives an effective way of visualizing regions where the field is coherent, but where the field varies significantly along the line of sight, the orientation pattern is irregular and difficult to interpret.

magnetic fields in the filaments and their background have an ordered component with a mean orientation inferred from *Planck* polarization data. However, the mean magnetic field in the filaments does not have the same orientation as in the background, with a different configuration in all three cases examined. The magnetic field in a massive star-forming region, the Rosette Nebula and parent molecular cloud, is analysed in Planck Collaboration Int. XXXIV (2016), combining Faraday rotation measures from the ionized gas with dust polarized emission from the swept-up shell. This same methodology and

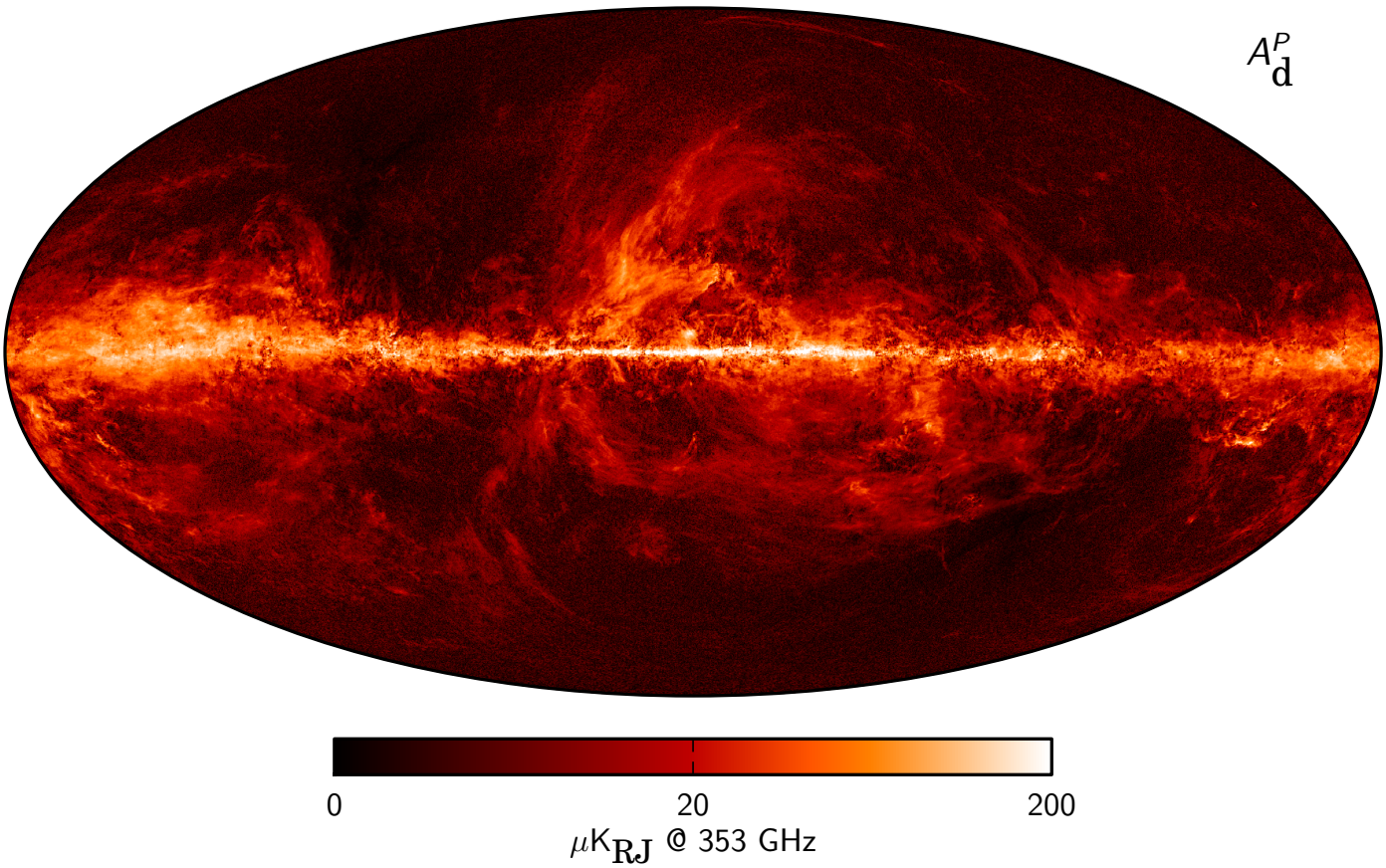


**Fig. 24.** Dust polarization amplitude map, $P = \sqrt{Q^2 + U^2}$, at 353 GHz, smoothed to an angular resolution of 10′, produced by the diffuse component-separation process described in Planck Collaboration X (2016) using *Planck* and WMAP data.

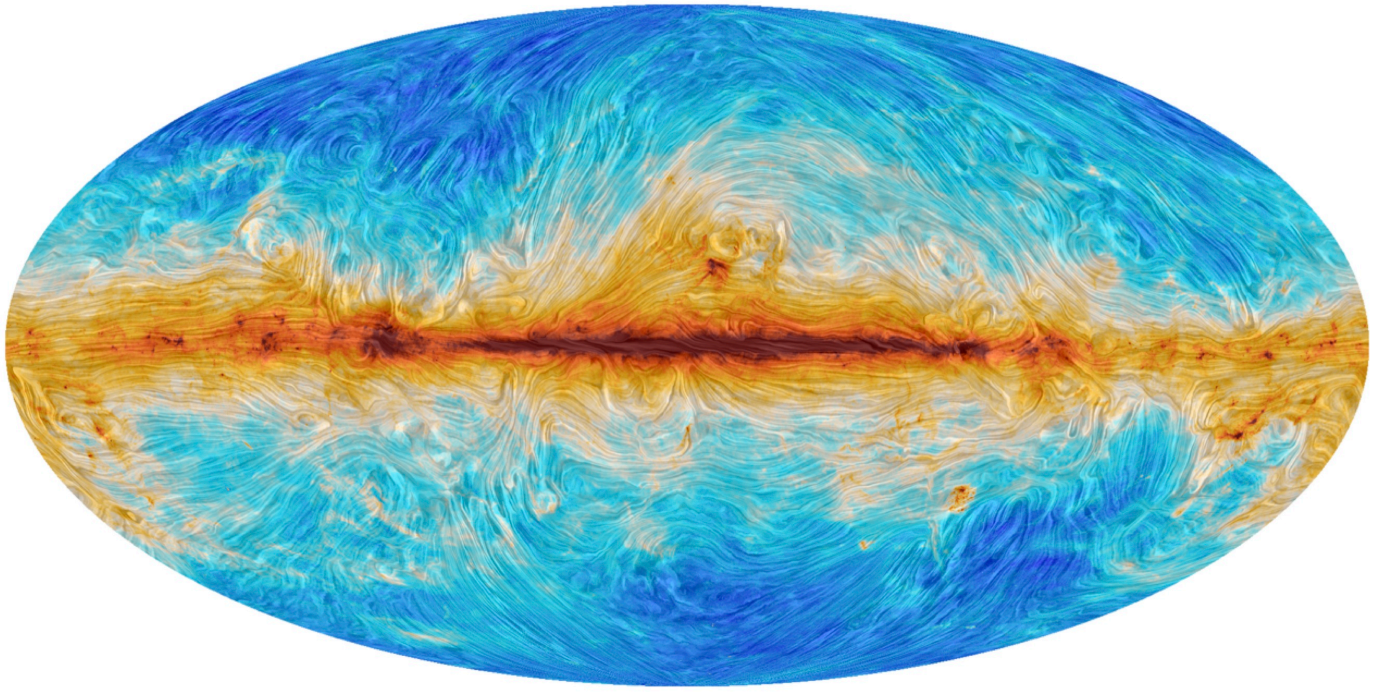

**Fig. 25.** All-sky view of the angle of polarization at 353 GHz, rotated by 90° to indicate the direction of the Galactic magnetic field projected on the plane of the sky and presented as in Fig. 23.

modelling framework could be used to study the field structure in a sample of massive star-forming regions.

#### 11.2.3. Dust polarization properties

Galactic interstellar dust consists of components with different sizes and compositions, and consequently different polarization properties. The relatively large grains that are in thermal equilibrium and emit the radiation seen by *Planck* in the submillimetre also extinguish and polarize starlight in the visible (e.g., Martin 2007). Comparison of polarized emission and starlight polarization on lines of sight probed by stars provides insight into the properties of polarizing grains. In Planck Collaboration Int. XXI (2015) we specifically use $P$ and $I$ in the *Planck* 353 GHz channel, stellar polarization observations in the $V$ band, the degree of polarization, $p_V$, and the optical depth to the star, $\tau_V$. Lines of sight through the diffuse interstellar medium are selected with comparable values of the column density as estimated at submillimetre and visible wavelengths, and with polarization directions in emission and extinction that are close to orthogonal. Through correlations involving many lines of sight two ratios are determined, $R_{S/V} = (P/I)/(p_V/\tau_V)$ and $R_{P/p} = P/p_V$, the latter focusing directly on the polarization properties of the grains contributing to polarization. The first ratio, $R_{S/V}$, is compatible with predictions based on a range of dust models that have been developed for the diffuse interstellar medium (e.g., Martin 2007; Draine & Fraisse 2009). This estimate provides new empirical validation of many of the common underlying assumptions of the models, but is not very discriminating among them. The second ratio, $R_{P/p}$, is higher than model predictions by a factor of about 2.5. A comparable difference between data and model is observed for $I/\tau_V$ (Planck Collaboration Int. XXIX 2016). To address this, changes will be needed in the modelled optical properties of the large dust grains contributing to the submillimetre emission and polarization.

The spectral dependence at submillimetre wavelengths is also important for constraining dust models. In Planck Collaboration Int. XXII (2015) the *Planck* and WMAP data are combined to characterize the frequency dependence of emission that is spatially correlated with dust emission at 353 GHz, for both intensity and polarization, in a consistent manner. At $\nu \geq 100$ GHz, the mean spectral energy distribution (SED) of the correlated emission is well fit by a modified blackbody spectrum, for which the mean dust temperature of 19.6 K (derived from an SED fit of the dust total intensity up to 3000 GHz $= 100\,\mu$m) is adopted. It is found that the opacity has a spectral index of $1.59 \pm 0.02$ for polarization and $1.51 \pm 0.01$ for intensity. The difference between the two spectral indices is small but significant. It might result from differences in polarization efficiency among different components of interstellar dust. Results from Planck Collaboration Int. XXII (2015) also show that the spectral energy distribution increases with decreasing frequency at $\nu < 60$ GHz, for both intensity and polarization. The rise of the polarization SED towards low frequency might be accounted for by a synchrotron component correlated with dust, with no need for any polarization of the anomalous microwave emission.

#### 11.2.4. Polarized dust and the CMB

The polarized thermal emission from diffuse Galactic dust is the main foreground present in measurements of the polarization of the CMB at frequencies above 70 GHz. The *Planck* sky coverage, spectral coverage, and sensitivity are all important for component separation of the polarization data. The polarized dust angular power spectra $C_\ell^{EE}$ and $C_\ell^{BB}$ are measured in Planck Collaboration Int. XXX (2016) over the multipole range $40 < \ell < 600$ and well away from the Galactic plane, providing a precise characterization of the dust foreground for CMB polarization.

The polarization power spectra of the dust are well-described by power laws in multipole, $C_\ell \propto \ell^\alpha$, with exponents $\alpha = -2.42 \pm 0.02$ for both the $EE$ and $BB$ spectra. The amplitudes of the polarization power spectra are observed to scale with the average dust brightness as $\langle I \rangle^{1.9}$, similar to the scaling found earlier (Miville-Deschênes et al. 2007). The frequency dependence of the power spectra for polarized thermal dust emission is consistent with that found for the modified blackbody emission in Planck Collaboration Int. XXII (2015). A systematic difference is discovered between the amplitudes of the Galactic $B$- and $E$-modes, such that $C_\ell^{BB}/C_\ell^{EE} = 0.5$. There is additional information coming from the dust $TE$ and $TB$ spectra. These general properties apply at intermediate and high Galactic latitudes in regions with low dust column density. The data show that there are no windows in the sky where primordial CMB $B$-mode polarization can be measured without subtraction of polarized dust emission.

## 12. Summary and conclusions

This paper is an overview of the *Planck* 2015 release, summarizing the main features of the products being released and the main scientific conclusions that we draw from them. Some highlights of this release are listed below.

- Data from the entire mission are now used, including both temperature and polarization, and significant improvements have been made in the understanding of beams, pointing, calibration, and systematic errors. As a result, the new products are less noisy, but even more importantly they are much better understood and the overall level of confidence is significantly increased.
- The residual systematics in the *Planck* 2015 polarization maps have been dramatically reduced compared to 2013, by as much as two orders of magnitude in some cases. Nevertheless, on angular scales greater than 10°, systematic errors in the polarization maps between 100 and 217 GHz are still non-negligible compared to the expected cosmological signal. It was not possible, for this data release, to fully characterize the large-scale residuals due to these systematic errors from the data or from simulations. Therefore all results published by the Planck Collaboration in 2015 based on CMB polarization maps use maps that have been high-pass filtered to remove structure on large angular scales. Users of the *Planck* CMB maps are warned that they are not generally usable for cosmological analysis at $\ell < 30$. Nevertheless, our polarization data are already making important contributions in a variety of analyses. More specifically, we are able to use the $TE$ and $EE$ angular power spectra at small scales (and to a more limited extent, at large angular scales) over the full sky, reaching the expected sensitivity. This allows us to estimate cosmological parameters independently of $TT$, and in combination with $TT$.
- A large set of simulations accompanies the release, including up to 10 000 realizations of signal and noise; this has been used to test and verify methods of analysis and to estimate uncertainties.

- We measure the amplitude and direction of the Solar dipole to the best precision so far.
- One of the most notable improvements in this release is that LFI, HFI, and WMAP now agree on the amplitude of fluctuations in the CMB to within a few tenths of a percent on angular scales from the dipole through the first acoustic peak.
- At large angular scales, we are now able to use *Planck*-only products to carry out cosmological analysis. Specifically, we can estimate the optical depth of reionization, $\tau$, independently of other experiments. The value of $\tau$ is smaller than found in previous determination, implying later reionization.
- Foregrounds can be separated effectively over larger areas of the sky than in the 2013 release, allowing more sky to be used for cosmology, and producing high-quality maps of synchrotron, free-free, spinning dust, thermal dust, and CO emission.
- Our 2015 results for cosmology are consistent with our 2013 results, but with smaller uncertainties, and covering a greater range of science implications.
- Our best-fit 2015 cosmological parameters confirm the basic 6-parameter ΛCDM scenario that we determined in 2013. There is no compelling evidence for any extensions to the 6-parameter model, or any need for new physics. Depending somewhat on the precise data combinations used, five of the six parameters are now measured to better than 1% precision. Areas that were in "tension" in 2013 ($\sigma_8$ and weak galaxy lensing) remain in tension today, although the disagreement is lessened when only particular subsets of the external data are considered.
- Using only *Planck* data, we find that the Universe is flat to 0.7% ($1\sigma$). Including BAO data, the constraint tightens to a remarkable 0.25%.
- Using the *Planck* temperature data over the whole sky, together with our recent work combining *Planck* and BICEP2/Keck data, we have obtained the best current upper limits on the tensor-to-scalar ratio obtained to date.
- Improved limits on primordial non-Gaussianity ($f_{\rm NL}$) are about 30% tighter than before, reaching the expected sensitivity of *Planck* when including polarization.
- Models of inflation are more tightly constrained than ever before, with the simplest $\phi^n$ models being ruled out for $n \geq 2$.
- We have obtained the most restrictive limits yet on the amplitude of primordial magnetic fields.
- *Planck*'s measurement of lensing of the CMB has the highest signal-to-noise ratio yet achieved, $40\sigma$.
- The second *Planck* catalogues of compact sources, SZ clusters, and Galactic cold clumps, are larger than the previous ones and better-characterized in terms of completeness and reliability.

*Planck* continues to provide a rich harvest of data for cosmology and astrophysics.

*Acknowledgements.* Planck is a project of the European Space Agency in cooperation with the scientific community, which started in 1993. ESA led the project, developed the satellite, integrated the payload into it, and launched and operated the satellite. Two Consortia, comprising around 100 scientific institutes within Europe, the USA, and Canada, and funded by agencies from the participating countries, developed and operated the scientific instruments LFI and HFI. The Consortia are also responsible for scientific processing of the acquired data. The Consortia are led by the Principal Investigators: J.-L. Puget in France for HFI (funded principally by CNES and CNRS/INSU-IN2P3) and N. Mandolesi in Italy for LFI (funded principally via ASI). NASA's US Planck Project, based at JPL and involving scientists at many US institutions, contributes significantly to the efforts of these two Consortia. A third Consortium, led by H.U. Norgaard-Nielsen and supported by the Danish Natural Research Council, contributed to the reflector programme. These three Consortia, together with ESA's Planck Science Office, form the Planck Collaboration. A description of the Planck Collaboration and a list of its members, indicating which technical or scientific activities they have been involved in, can be found at http://www.cosmos.esa.int/web/planck/planck-collaboration. The Planck Collaboration acknowledges the support of: ESA; CNES and CNRS/INSU-IN2P3-INP (France); ASI, CNR, and INAF (Italy); NASA and DoE (USA); STFC and UKSA (UK); CSIC, MINECO, JA, and RES (Spain); Tekes, AoF, and CSC (Finland); DLR and MPG (Germany); CSA (Canada); DTU Space (Denmark); SER/SSO (Switzerland); RCN (Norway); SFI (Ireland); FCT/MCTES (Portugal); ERC and PRACE (EU). We thank Diego Falceta-Gonçalves for providing the technique for making the line-integral-convolution maps presented in Figs. 23 and 25.

## References

Bennett, C. L., Larson, D., Weiland, J. L., et al. 2013, ApJ, 208, 20
Benoît, A., Ade, P., Amblard, A., et al. 2004, A&A, 424, 571
Bersanelli, M., Mandolesi, N., Butler, R. C., et al. 2010, A&A, 520, A4
Béthermin, M., Daddi, E., Magdis, G., et al. 2012, ApJ, 757, L23
BICEP2 Collaboration 2014, Phys. Rev. Lett., 112, 241101
BICEP2/Keck Array and Planck Collaborations 2015, Phys. Rev. Lett., 114, 101301
Bond, J. R., Contaldi, C., & Pogosyan, D. 2003, Roy. Soc. London Philos. Trans. Ser. A, 361, 2435
Cabral, B., & Leedom, L. C. 1993, in Special Interest Group on GRAPHics and Interactive Techniques Proceedings, 263
Cardoso, J., Martin, M., Delabrouille, J., Betoule, M., & Patanchon, G. 2008, special issue on Signal Processing for Astronomical and Space Research Applications, IEEE J. Selected Topics in Signal Processing, 2, 735
Corasaniti, P. S., & Melchiorri, A. 2008, Phys. Rev. D, 77, 103507
de Bernardis, P., Ade, P. A. R., Bock, J. J., et al. 2002, ApJ, 564, 559
Delabrouille, J., Cardoso, J.-F., & Patanchon, G. 2003, MNRAS, 346, 1089
Delabrouille, J., Cardoso, J., Le Jeune, M., et al. 2009, A&A, 493, 835
Delabrouille, J., Betoule, M., Melin, J.-B., et al. 2013, A&A, 553, A96
Draine, B. T., & Fraisse, A. A. 2009, ApJ, 696, 1
Durrer, R., Novosyadlyj, B., & Apunevych, S. 2003, ApJ, 583, 33
Eriksen, H. K., Hansen, F. K., Banday, A. J., Górski, K. M., & Lilje, P. B. 2004, ApJ, 605, 14
Eriksen, H. K., Dickinson, C., Lawrence, C. R., et al. 2006, ApJ, 641, 665
Eriksen, H. K., Jewell, J. B., Dickinson, C., et al. 2008, ApJ, 676, 10
Fernández-Cobos, R., Vielva, P., Barreiro, R. B., & Martínez-González, E. 2012, MNRAS, 420, 2162
Górski, K. M., Hivon, E., Banday, A. J., et al. 2005, ApJ, 622, 759
Granett, B. R., Neyrinck, M. C., & Szapudi, I. 2008, ApJ, 683, L99
Hamaker, J. P., & Bregman, J. D. 1996, A&AS, 117, 161
Hancock, S., & Rocha, G. 1997, in Microwave Background Anisotropies, eds. F. R. Bouchet, R. Gispert, B. Guiderdoni, & J. Trân Thanh Vân, 179
Haslam, C. G. T., Salter, C. J., Stoffel, H., & Wilson, W. E. 1982, A&AS, 47, 1
Heeschen, D. S., & Howard, W. E. 1974, in Trans. IAU, Vol. XVB, Proc. 1973, General Assembly, eds. G. Contopoulos, & A. Jappel (Dordrecht: Reidel), 165
Hildebrand, R. H., Kirby, L., Dotson, J. L., Houde, M., & Vaillancourt, J. E. 2009, ApJ, 696, 567
Hinshaw, G., Nolta, M. R., Bennett, C. L., et al. 2007, ApJS, 170, 288
Hinshaw, G., Weiland, J. L., Hill, R. S., et al. 2009, ApJS, 180, 225
Hu, W., Hedman, M. M., & Zaldarriaga, M. 2003, Phys. Rev. D, 67, 043004
Hurier, G., Macías-Pérez, J. F., & Hildebrandt, S. R. 2013, A&A, 558, A118
Iacobelli, M., Burkhart, B., Haverkorn, M., et al. 2014, A&A, 566, A5
Jarosik, N., Bennett, C. L., Dunkley, J., et al. 2011, ApJS, 192, 14
Jones, W. C., Ade, P. A. R., Bock, J. J., et al. 2006, ApJ, 647, 823
Keihänen, E., Keskitalo, R., Kurki-Suonio, H., Poutanen, T., & Sirviö, A. 2010, A&A, 510, A57
Knox, L., & Page, L. 2000, Phys. Rev. Lett., 85, 1366
Koch, P. M., Tang, Y.-W., & Ho, P. T. P. 2010, ApJ, 721, 815
Lamarre, J., Puget, J., Ade, P. A. R., et al. 2010, A&A, 520, A9
Leahy, J. P., Bersanelli, M., D'Arcangelo, O., et al. 2010, A&A, 520, A8
Martin, P. G. 2007, in EAS Pub. Ser. 23, eds. M.-A. Miville-Deschênes, & F. Boulanger, 165
Matthews, B. C., McPhee, C. A., Fissel, L. M., & Curran, R. L. 2009, ApJS, 182, 143
Matthews, T. G., Ade, P. A. R., Angilè, F. E., et al. 2014, ApJ, 784, 116
Melin, J.-B., & Bartlett, J. G. 2015, A&A, 578, A21
Mennella, A., Butler, R. C., Curto, A., et al. 2011, A&A, 536, A3
Mertsch, P., & Sarkar, S. 2013, JCAP, 6, 41
Mitra, S., Rocha, G., Górski, K. M., et al. 2011, ApJS, 193, 5
Miville-Deschênes, M., & Lagache, G. 2005, ApJS, 157, 302

Miville-Deschênes, M.-A., Lagache, G., Boulanger, F., & Puget, J.-L. 2007, A&A, 469, 595
Montier, L. A., Pelkonen, V., Juvela, M., Ristorcelli, I., & Marshall, D. J. 2010, A&A, 522, A83
Oppermann, N., Junklewitz, H., Robbers, G., et al. 2012, A&A, 542, A93
Page, L., Nolta, M. R., Barnes, C., et al. 2003, ApJS, 148, 233
Planck Collaboration 2005, ESA publication ESA-SCI(2005)/01 [arXiv:astro-ph/0604069]
Planck Collaboration 2015, The Explanatory Supplement to the *Planck* 2015 results, http://wiki.cosmos.esa.int/planckpla/index.php/Main_Page (ESA)
Planck Collaboration I. 2011, A&A, 536, A1
Planck Collaboration VII. 2011, A&A, 536, A7
Planck Collaboration XIII. 2011, A&A, 536, A13
Planck Collaboration XIV. 2011, A&A, 536, A14
Planck Collaboration XXII. 2011, A&A, 536, A22
Planck Collaboration XXIII. 2011, A&A, 536, A23
Planck Collaboration I. 2014, A&A, 571, A1
Planck Collaboration II. 2014, A&A, 571, A2
Planck Collaboration IV. 2014, A&A, 571, A4
Planck Collaboration V. 2014, A&A, 571, A5
Planck Collaboration VI. 2014, A&A, 571, A6
Planck Collaboration VII. 2014, A&A, 571, A7
Planck Collaboration XI. 2014, A&A, 571, A11
Planck Collaboration XIII. 2014, A&A, 571, A13
Planck Collaboration XIV. 2014, A&A, 571, A14
Planck Collaboration XV. 2014, A&A, 571, A15
Planck Collaboration XVI. 2014, A&A, 571, A16
Planck Collaboration XVII. 2014, A&A, 571, A17
Planck Collaboration XIX. 2014, A&A, 571, A19
Planck Collaboration XXI. 2014, A&A, 571, A21
Planck Collaboration XXII. 2014, A&A, 571, A22
Planck Collaboration XXVI. 2014, A&A, 571, A26
Planck Collaboration XXVII. 2014, A&A, 571, A27
Planck Collaboration XXVIII. 2014, A&A, 571, A28
Planck Collaboration XXIX. 2014, A&A, 571, A29
Planck Collaboration XXXI. 2014, A&A, 571, A31
Planck Collaboration I. 2016, A&A, 594, A1
Planck Collaboration II. 2016, A&A, 594, A2
Planck Collaboration III. 2016, A&A, 594, A3
Planck Collaboration IV. 2016, A&A, 594, A4
Planck Collaboration V. 2016, A&A, 594, A5
Planck Collaboration VI. 2016, A&A, 594, A6
Planck Collaboration VII. 2016, A&A, 594, A7
Planck Collaboration VIII. 2016, A&A, 594, A8
Planck Collaboration IX. 2016, A&A, 594, A9
Planck Collaboration X. 2016, A&A, 594, A10
Planck Collaboration XI. 2016, A&A, 594, A11
Planck Collaboration XII. 2016, A&A, 594, A12
Planck Collaboration XIII. 2016, A&A, 594, A13
Planck Collaboration XIV. 2016, A&A, 594, A14
Planck Collaboration XV. 2016, A&A, 594, A15
Planck Collaboration XVI. 2016, A&A, 594, A16
Planck Collaboration XVII. 2016, A&A, 594, A17
Planck Collaboration XVIII. 2016, A&A, 594, A18
Planck Collaboration XIX. 2016, A&A, 594, A19
Planck Collaboration XX. 2016, A&A, 594, A20
Planck Collaboration XXI. 2016, A&A, 594, A21
Planck Collaboration XXII. 2016, A&A, 594, A22
Planck Collaboration XXIII. 2016, A&A, 594, A23
Planck Collaboration XXIV. 2016, A&A, 594, A24
Planck Collaboration XXV. 2016, A&A, 594, A25
Planck Collaboration XXVI. 2016, A&A, 594, A26
Planck Collaboration XXVII. 2016, A&A, 594, A27
Planck Collaboration XXVIII. 2016, A&A, 594, A28
Planck Collaboration Int. XIX. 2015, A&A, 576, A104
Planck Collaboration Int. XX. 2015, A&A, 576, A105
Planck Collaboration Int. XXI. 2015, A&A, 576, A106
Planck Collaboration Int. XXII. 2015, A&A, 576, A107
Planck Collaboration Int. XXIX. 2016, A&A, 586, A132
Planck Collaboration Int. XXX. 2016, A&A, 586, A133
Planck Collaboration Int. XXXII. 2016, A&A, 586, A135
Planck Collaboration Int. XXXIII. 2016, A&A, 586, A136
Planck Collaboration Int. XXXIV. 2016, A&A, 586, A137
Planck Collaboration Int. XXXV. 2016, A&A, 586, A138
Planck HFI Core Team 2011, A&A, 536, A4
Pryke, C., Ade, P., Bock, J., et al. 2009, ApJ, 692, 1247
Readhead, A. C. S., Myers, S. T., Pearson, T. J., et al. 2004, Science, 306, 836
Remazeilles, M., Delabrouille, J., & Cardoso, J.-F. 2011, MNRAS, 410, 2481
Scott, D., & White, M. 1994, in CMB Anisotropies Two Years after COBE: Observations, Theory and the Future, ed. L. M. Krauss, 214
Tauber, J. A., Mandolesi, N., Puget, J., et al. 2010, A&A, 520, A1
Tristram, M., Filliard, C., Perdereau, O., et al. 2011, A&A, 534, A88
Vidal, M., Dickinson, C., Davies, R. D., & Leahy, J. P. 2015, MNRAS, 432, 656
von der Linden, A., Mantz, A., Allen, S. W., et al. 2014, MNRAS, 443, 1973
Ward-Thompson, D., Sen, A. K., Kirk, J. M., & Nutter, D. 2009, MNRAS, 398, 394

[1] APC, AstroParticule et Cosmologie, Université Paris Diderot, CNRS/IN2P3, CEA/lrfu, Observatoire de Paris, Sorbonne Paris Cité, 10 rue Alice Domon et Léonie Duquet, 75205 Paris Cedex 13, France
[2] Aalto University Metsähovi Radio Observatory and Dept of Radio Science and Engineering, PO Box 13000, 00076 Aalto, Finland
[3] Aalto University Metsähovi Radio Observatory, PO Box 13000, 00076 Aalto, Finland
[4] Academy of Sciences of Tatarstan, Bauman Str., 20, Kazan, 420111, Republic of Tatarstan, Russia
[5] African Institute for Mathematical Sciences, 6-8 Melrose Road, Muizenberg, Cape Town, South Africa
[6] Agenzia Spaziale Italiana Science Data Center, Via del Politecnico snc, 00133, Roma, Italy
[7] Aix-Marseille Université, CNRS, LAM (Laboratoire d'Astrophysique de Marseille) UMR 7326, 13388, Marseille, France
[8] Aix Marseille Université, Centre de Physique Théorique, 163 avenue de Luminy, 13288, Marseille, France
[9] Astrophysics Group, Cavendish Laboratory, University of Cambridge, J J Thomson Avenue, Cambridge CB3 0HE, UK
[10] Astrophysics & Cosmology Research Unit, School of Mathematics, Statistics & Computer Science, University of KwaZulu-Natal, Westville Campus, Private Bag X54001, Durban 4000, South Africa
[11] Atacama Large Millimeter/submillimeter Array, ALMA Santiago Central Offices, Alonso de Cordova 3107, Vitacura, Casilla 763 0355, Santiago, Chile
[12] CGEE, SCS Qd 9, Lote C, Torre C, 4° andar, Ed. Parque Cidade Corporate, CEP 70308-200, Brasília, DF, Brazil
[13] CITA, University of Toronto, 60 St. George St., Toronto, ON M5S 3H8, Canada
[14] CNRS, IRAP, 9 Av. colonel Roche, BP 44346, 31028 Toulouse Cedex 4, France
[15] CRANN, Trinity College, Dublin, Ireland
[16] California Institute of Technology, Pasadena, California, USA
[17] Centre for Theoretical Cosmology, DAMTP, University of Cambridge, Wilberforce Road, Cambridge CB3 0WA, UK
[18] Centro de Estudios de Física del Cosmos de Aragón (CEFCA), Plaza San Juan, 1, Planta 2, 44001, Teruel, Spain
[19] Computational Cosmology Center, Lawrence Berkeley National Laboratory, Berkeley, California, USA
[20] Consejo Superior de Investigaciones Científicas (CSIC), Madrid, Spain
[21] DSM/Irfu/SPP, CEA-Saclay, 91191 Gif-sur-Yvette Cedex, France
[22] DTU Space, National Space Institute, Technical University of Denmark, Elektrovej 327, 2800 Kgs. Lyngby, Denmark
[23] Département de Physique Théorique, Université de Genève, 24 quai E. Ansermet, 1211 Genève 4, Switzerland
[24] Dark Cosmology Centre, Niels Bohr Institute, University of Copenhagen, Juliane Maries Vej 30, 2100 Copenhagen, Denmark
[25] Departamento de Astrofísica, Universidad de La Laguna (ULL), 38206 La Laguna, Tenerife, Spain
[26] Departamento de Física, Universidad de Oviedo, Avda. Calvo Sotelo s/n, Oviedo, Spain
[27] Departamento de Matemáticas, Estadística y Computación, Universidad de Cantabria, Avda. de los Castros s/n, Santander, Spain
[28] Departamento de Matemáticas, Universidad de Oviedo, Avda. Calvo Sotelo s/n, Oviedo, Spain
[29] Department of Astronomy and Astrophysics, University of Toronto, 50 Saint George Street, Toronto, Ontario, Canada

[30] Department of Astronomy and Geodesy, Kazan Federal University, Kremlevskaya Str., 18, Kazan, 420008, Russia
[31] Department of Astrophysics/IMAPP, Radboud University Nijmegen, PO Box 9010, 6500 GL Nijmegen, The Netherlands
[32] Department of Physics & Astronomy, University of British Columbia, 6224 Agricultural Road, Vancouver, British Columbia, Canada
[33] Department of Physics and Astronomy, Dana and David Dornsife College of Letter, Arts and Sciences, University of Southern California, Los Angeles, CA 90089, USA
[34] Department of Physics and Astronomy, Johns Hopkins University, Bloomberg Center 435, 3400 N. Charles St., Baltimore, MD 21218, USA
[35] Department of Physics and Astronomy, University College London, London WC1E 6BT, UK
[36] Department of Physics and Astronomy, University of Sussex, Brighton BN1 9QH, UK
[37] Department of Physics, Florida State University, Keen Physics Building, 77 Chieftan Way, Tallahassee, Florida, USA
[38] Department of Physics, Gustaf Hällströmin katu 2a, University of Helsinki, Helsinki, Finland
[39] Department of Physics, Princeton University, Princeton, New Jersey, USA
[40] Department of Physics, University of Alberta, 11322-89 Avenue, Edmonton, Alberta, T6G 2G7, Canada
[41] Department of Physics, University of California, Berkeley, California, USA
[42] Department of Physics, University of California, One Shields Avenue, Davis, California, USA
[43] Department of Physics, University of California, Santa Barbara, California, USA
[44] Department of Physics, University of Illinois at Urbana-Champaign, 1110 West Green Street, Urbana, Illinois, USA
[45] Dipartimento di Fisica e Astronomia G. Galilei, Università degli Studi di Padova, via Marzolo 8, 35131 Padova, Italy
[46] Dipartimento di Fisica e Astronomia, Alma Mater Studiorum, Università degli Studi di Bologna, Viale Berti Pichat 6/2, 40127 Bologna, Italy
[47] Dipartimento di Fisica e Scienze della Terra, Università di Ferrara, Via Saragat 1, 44122 Ferrara, Italy
[48] Dipartimento di Fisica, Università La Sapienza, P.le A. Moro 2, Roma, Italy
[49] Dipartimento di Fisica, Università degli Studi di Milano, Via Celoria, 16, Milano, Italy
[50] Dipartimento di Fisica, Università degli Studi di Trieste, via A. Valerio 2, Trieste, Italy
[51] Dipartimento di Fisica, Università di Roma Tor Vergata, Via della Ricerca Scientifica 1, Roma, Italy
[52] Dipartimento di Matematica, Università di Roma Tor Vergata, Via della Ricerca Scientifica 1, Roma, Italy
[53] Discovery Center, Niels Bohr Institute, Blegdamsvej 17, Copenhagen, Denmark
[54] Discovery Center, Niels Bohr Institute, Copenhagen University, Blegdamsvej 17, Copenhagen, Denmark
[55] European Southern Observatory, ESO Vitacura, Alonso de Cordova 3107, Vitacura, Casilla 19001, Santiago, Chile
[56] European Space Agency, ESAC, Camino bajo del Castillo s/n, Urbanización Villafranca del Castillo, Villanueva de la Cañada, Madrid, Spain
[57] European Space Agency, ESAC, Planck Science Office, Camino bajo del Castillo s/n, Urbanización Villafranca del Castillo, Villanueva de la Cañada, Madrid, Spain
[58] European Space Agency, ESTEC, Keplerlaan 1, 2201 AZ Noordwijk, The Netherlands
[59] Finnish Centre for Astronomy with ESO (FINCA), University of Turku, Väisäläntie 20, 21500 Piikkiö, Finland
[60] GEPI, Observatoire de Paris, Section de Meudon, 5 place J. Janssen, 92195 Meudon Cedex, France
[61] Gran Sasso Science Institute, INFN, viale F. Crispi 7, 67100 L'Aquila, Italy
[62] HGSFP and University of Heidelberg, Theoretical Physics Department, Philosophenweg 16, 69120, Heidelberg, Germany
[63] Haverford College Astronomy Department, 370 Lancaster Avenue, Haverford, Pennsylvania, USA
[64] Helsinki Institute of Physics, Gustaf Hällströmin katu 2, University of Helsinki, Helsinki, Finland
[65] ICTP South American Institute for Fundamental Research, Instituto de Física Teórica, Universidade Estadual Paulista, São Paulo, Brazil
[66] INAF – Osservatorio Astrofisico di Catania, Via S. Sofia 78, Catania, Italy
[67] INAF – Osservatorio Astronomico di Padova, Vicolo dell'Osservatorio 5, Padova, Italy
[68] INAF – Osservatorio Astronomico di Roma, via di Frascati 33, Monte Porzio Catone, Italy
[69] INAF – Osservatorio Astronomico di Trieste, Via G.B. Tiepolo 11, Trieste, Italy
[70] INAF/IASF Bologna, Via Gobetti 101, Bologna, Italy
[71] INAF/IASF Milano, Via E. Bassini 15, Milano, Italy
[72] INFN, Sezione di Bologna, viale Berti Pichat 6/2, 40127 Bologna, Italy
[73] INFN, Sezione di Ferrara, Via Saragat 1, 44122 Ferrara, Italy
[74] INFN, Sezione di Roma 1, Università di Roma Sapienza, Piazzale Aldo Moro 2, 00185 Roma, Italy
[75] INFN, Sezione di Roma 2, Università di Roma Tor Vergata, Via della Ricerca Scientifica 1, Roma, Italy
[76] INFN/National Institute for Nuclear Physics, Via Valerio 2, 34127 Trieste, Italy
[77] IPAG: Institut de Planétologie et d'Astrophysique de Grenoble, Université Grenoble Alpes, IPAG; CNRS, IPAG, 38000 Grenoble, France
[78] ISDC, Department of Astronomy, University of Geneva, Ch. d'Ecogia 16, 1290 Versoix, Switzerland
[79] IUCAA, Post Bag 4, Ganeshkhind, Pune University Campus, Pune 411 007, India
[80] Imperial College London, Astrophysics group, Blackett Laboratory, Prince Consort Road, London, SW7 2AZ, UK
[81] Infrared Processing and Analysis Center, California Institute of Technology, Pasadena, CA 91125, USA
[82] Institut Néel, CNRS, Université Joseph Fourier Grenoble I, 25 rue des Martyrs, Grenoble, France
[83] Institut Universitaire de France, 103 bd Saint-Michel, 75005 Paris, France
[84] Institut d'Astrophysique Spatiale, CNRS, Univ. Paris-Sud, Université Paris-Saclay, Bât. 121, 91405 Orsay Cedex, France
[85] Institut d'Astrophysique de Paris, CNRS (UMR 7095), 98bis boulevard Arago, 75014 Paris, France
[86] Institut für Theoretische Teilchenphysik und Kosmologie, RWTH Aachen University, 52056 Aachen, Germany
[87] Institute for Space Sciences, Bucharest-Magurale, Romania
[88] Institute of Astronomy, University of Cambridge, Madingley Road, Cambridge CB3 0HA, UK
[89] Institute of Theoretical Astrophysics, University of Oslo, Blindern, Oslo, Norway
[90] Instituto Nacional de Astrofísica, Óptica y Electrónica (INAOE), Apartado Postal 51 y 216, 72000 Puebla, México
[91] Instituto de Astrofísica de Canarias, C/Vía Láctea s/n, La Laguna, Tenerife, Spain
[92] Instituto de Física de Cantabria (CSIC-Universidad de Cantabria), Avda. de los Castros s/n, Santander, Spain
[93] Istituto Nazionale di Astrofisica – Osservatorio Astronomico di Roma, Via Frascati 33, 00040 Monte Porzio Catone (RM), Italy
[94] Istituto Nazionale di Fisica Nucleare, Sezione di Padova, via Marzolo 8, 35131 Padova, Italy
[95] Jet Propulsion Laboratory, California Institute of Technology, 4800 Oak Grove Drive, Pasadena, California, USA
[96] Jodrell Bank Centre for Astrophysics, Alan Turing Building, School of Physics and Astronomy, The University of Manchester, Oxford Road, Manchester, M13 9PL, UK

[97] Kavli Institute for Cosmological Physics, University of Chicago, Chicago, IL 60637, USA
[98] Kavli Institute for Cosmology Cambridge, Madingley Road, Cambridge, CB3 0HA, UK
[99] Kazan Federal University, 18 Kremlyovskaya St., Kazan 420008, Russia
[100] LAL, Université Paris-Sud, CNRS/IN2P3, Orsay, France
[101] LERMA, CNRS, Observatoire de Paris, 61 Avenue de l'Observatoire, Paris, France
[102] LESIA, Observatoire de Paris, CNRS, UPMC, Université Paris-Diderot, 5 Place J. Janssen, 92195 Meudon, France
[103] Laboratoire AIM, IRFU/Service d'Astrophysique - CEA/DSM - CNRS - Université Paris Diderot, Bât. 709, CEA-Saclay, 91191 Gif-sur-Yvette Cedex, France
[104] Laboratoire Traitement et Communication de l'Information, CNRS (UMR 5141) and Télécom ParisTech, 46 rue Barrault, 75634 Paris Cedex 13, France
[105] Laboratoire de Physique Subatomique et Cosmologie, Université Grenoble-Alpes, CNRS/IN2P3, 53 rue des Martyrs, 38026 Grenoble Cedex, France
[106] Laboratoire de Physique Théorique, Université Paris-Sud 11 & CNRS, Bâtiment 210, 91405 Orsay, France
[107] Lawrence Berkeley National Laboratory, Berkeley, California, USA
[108] Lebedev Physical Institute of the Russian Academy of Sciences, Astro Space Centre, 84/32 Profsoyuznaya st., Moscow, GSP-7, 117997, Russia
[109] Leung Center for Cosmology and Particle Astrophysics, National Taiwan University, Taipei 10617, Taiwan
[110] Max-Planck-Institut für Astrophysik, Karl-Schwarzschild-Str. 1, 85741 Garching, Germany
[111] Max-Planck-Institut für Extraterrestrische Physik, Giessenbachstraße, 85748 Garching, Germany
[112] McGill Physics, Ernest Rutherford Physics Building, McGill University, 3600 rue University, Montréal, QC, H3A 2T8, Canada
[113] Moscow Institute of Physics and Technology, Institutsky per., 9, Dolgoprudny, 141700, Russia
[114] Mullard Space Science Laboratory, University College London, Surrey RH5 6NT, UK
[115] National University of Ireland, Department of Experimental Physics, Maynooth, Co. Kildare, Ireland
[116] Nicolaus Copernicus Astronomical Center, Bartycka 18, 00-716 Warsaw, Poland
[117] Niels Bohr Institute, Blegdamsvej 17, Copenhagen, Denmark
[118] Niels Bohr Institute, Copenhagen University, Blegdamsvej 17, Copenhagen, Denmark
[119] Nordita (Nordic Institute for Theoretical Physics), Roslagstullsbacken 23, 106 91 Stockholm, Sweden
[120] Optical Science Laboratory, University College London, Gower Street, London, UK
[121] Perimeter Institute for Theoretical Physics, Waterloo ON N2L 2Y5, Canada
[122] Physics Department, Shahid Beheshti University, Tehran, Iran
[123] SISSA, Astrophysics Sector, via Bonomea 265, 34136, Trieste, Italy
[124] SMARTEST Research Centre, Università degli Studi e-Campus, Via Isimbardi 10, Novedrate (CO), 22060, Italy
[125] School of Chemistry and Physics, University of KwaZulu-Natal, Westville Campus, Private Bag X54001, 4000 Durban, South Africa
[126] School of Physics and Astronomy, Cardiff University, Queens Buildings, The Parade, Cardiff, CF24 3AA, UK
[127] School of Physics and Astronomy, University of Nottingham, Nottingham NG7 2RD, UK
[128] Simon Fraser University, Department of Physics, 8888 University Drive, Burnaby BC, Canada
[129] Sorbonne Université-UPMC, UMR7095, Institut d'Astrophysique de Paris, 98bis Boulevard Arago, 75014 Paris, France
[130] Space Research Institute (IKI), Russian Academy of Sciences, Profsoyuznaya Str, 84/32, 117997 Moscow, Russia
[131] Space Sciences Laboratory, University of California, Berkeley, California, USA
[132] Special Astrophysical Observatory, Russian Academy of Sciences, Nizhnij Arkhyz, Zelenchukskiy region, 369167 Karachai-Cherkessian Republic, Russia
[133] Stanford University, Dept of Physics, Varian Physics Bldg, 382 Via Pueblo Mall, Stanford, California, USA
[134] Sterrewacht Leiden, PO Box 9513, 2300 RA Leiden, The Netherlands
[135] Sub-Department of Astrophysics, University of Oxford, Keble Road, Oxford OX1 3RH, UK
[136] Sydney Institute for Astronomy, School of Physics A28, University of Sydney, NSW 2006, Australia
[137] TÜBİTAK National Observatory, Akdeniz University Campus, 07058 Antalya, Turkey
[138] The Oskar Klein Centre for Cosmoparticle Physics, Department of Physics, Stockholm University, AlbaNova, 106 91 Stockholm, Sweden
[139] Theory Division, PH-TH, CERN, 1211 Geneva 23, Switzerland
[140] UPMC Univ Paris 06, UMR7095, 98bis Boulevard Arago, 75014 Paris, France
[141] Universität Heidelberg, Institut für Theoretische Astrophysik, Philosophenweg 12, 69120 Heidelberg, Germany
[142] Université Denis Diderot (Paris 7), 75205 Paris Cedex 13, France
[143] Université de Toulouse, UPS-OMP, IRAP, 31028 Toulouse Cedex 4, France
[144] Universities Space Research Association, Stratospheric Observatory for Infrared Astronomy, MS 232-11, Moffett Field, CA 94035, USA
[145] University Observatory, Ludwig Maximilian University of Munich, Scheinerstrasse 1, 81679 Munich, Germany
[146] University of Granada, Departamento de Física Teórica y del Cosmos, Facultad de Ciencias, Granada, Spain
[147] University of Granada, Instituto Carlos I de Física Teórica y Computacional, Granada, Spain
[148] University of Heidelberg, Institute for Theoretical Physics, Philosophenweg 16, 69120 Heidelberg, Germany
[149] W. W. Hansen Experimental Physics Laboratory, Kavli Institute for Particle Astrophysics and Cosmology, Department of Physics and SLAC National Accelerator Laboratory, Stanford University, Stanford, CA 94305, USA
[150] Warsaw University Observatory, Aleje Ujazdowskie 4, 00-478 Warszawa, Poland